A&A 469, 1151–1154 (2007)
DOI: 10.1051/0004-6361:20077492

Astronomy & Astrophysics

On understanding the meaning of $l = 2$ and 3 p-mode frequencies as measured by various helioseismic instruments *(Research Note)*

T. Appourchaux[1] and W. J. Chaplin[2]

[1] Institut d'Astrophysique Spatiale, Université Paris XI – CNRS, Bâtiment 121, 91405 Orsay Cedex, France
e-mail: Thierry.Appourchaux@ias.u-psud.fr
[2] School of Physics and Astronomy, University of Birmingham, Edgbaston, Birmingham B15 2TT, UK
e-mail: wjc@bison.ph.bham.ac.uk

Received 16 March 2007 / Accepted 28 April 2007

ABSTRACT

Aims. Frequencies of the low-degree p-mode oscillations of the Sun may be extracted either from data collected by instruments that make full-disc observations of the Sun as a star, or from data collected by instruments that resolve, or image, the Sun's surface onto many detector elements. The two methods can show marked differences in their sensitivity to modes having certain combinations of degree and azimuthal order. These different sensitivities lead to differences in measurements of the central frequencies of the modes, which must be properly accounted for if data from two different instruments are to be compared, or combined.
Methods. We perform an analytical derivation of the p-mode frequency offsets expected between contemporaneous Sun-as-a-star and resolved-Sun data.
Results. Here, we demonstrate that the empirical factors derived by Chaplin et al. (2004, A&A, 424, 713) are reproduced by our analysis, but with a more marked dependence upon the mode linewidth.

Key words. methods: data analysis – methods: statistical – Sun: helioseismology – Sun: oscillations

1. Introduction

Solar p-mode frequencies are used to make inference on the internal structure of the Sun. Modes characterized by degree l less than ∼4 are able to probe the core of the Sun. The frequencies of these modes are extracted either from data collected by instruments observing the Sun as a star (e.g., the ground-based BiSON (Chaplin et al. 1996) and the GOLF (Gabriel et al. 1995) and VIRGO/SPM (Fröhlich et al. 1995) instruments on board the *ESA/NASA* SOHO spacecraft), or from data collected by instruments that resolve, or image, the Sun's surface onto many detector elements (e.g., the ground-based GONG (Harvey et al. 1996), and the MDI (Scherrer et al. 1995) and VIRGO/LOI (Appourchaux et al. 1997) on SOHO). In order to exploit both types of data correctly, the user must be aware of crucial differences in the sensitivity of each method to the $2l + 1$ components of a mode.

The resolved, or imaged, observations can in principle provide high-quality data on all $2l + 1$ components of a mode. This allows estimates of the frequency centroids of the mode multiplets to be made. We call these estimates $\nu_{n,l}^{\rm RES}$. The Sun-as-a-star, or full-disc, data in contrast provide useful data on only $l + 1$ components of a mode. This is because the rotation axis of the Sun is always close to the plane of the sky: the disc-averaged Doppler velocity or intensity perturbations of modes of odd $l+m$ are then very small, rendering them unobservable in the Sun-as-a-star data. Because the Sun-as-a-star data do not "see" all the components, it is therefore not possible to estimate the frequency centroids of the multiplets. Estimated frequencies from the Sun-as-a-star, full-disc data, which we call $\nu_{n,l}^{\rm FD}$, are therefore expected to differ from their resolved-Sun counterparts.

Chaplin et al. (2004) discussed these issues at length, and expressed differences between the full-disc and resolved-Sun frequencies in terms of the even-a splitting coefficients, which are related to the surface activity, and an empirically derived coefficient, which fixed the contribution of the different m components to the fitted full-disc frequencies. Our aim in this paper is to provide an analytical derivation that can be used for any instrument.

2. Analytical derivation of the relation

Based upon the work of Chaplin et al. (2004), we derive estimates of the Sun-as-a-star, full-disc frequencies (FD) in terms of the estimated centroid frequencies from the resolved, imaging instruments (RES) and the even-a splitting coefficients, i.e.,

$$\nu_{n,l}^{\rm FD} = \nu_{n,l}^{\rm RES} + \sum_{i=2,4,6} a_i(n,l) C_i^l. \quad (1)$$

In the above, $\nu_{n,l}^{\rm FD}$ is the frequency obtained from full-disc instrument data; $\nu_{n,l}^{\rm RES}$ is the centroid frequency obtained from resolved, imaging instrument data; the $a_i(n,l)$ are the even-a splitting coefficients; and the C_i^l, which fix the contribution of different terms to the frequency differences, are coefficients that we wish to derive.

At $l = 2$, the multiplet frequency asymmetry parameter, as given in Chaplin et al. (2004), is the difference between the mean frequency of the $|m| = 2$ components and the frequency of the $m = 0$ component. It can be shown that this difference is

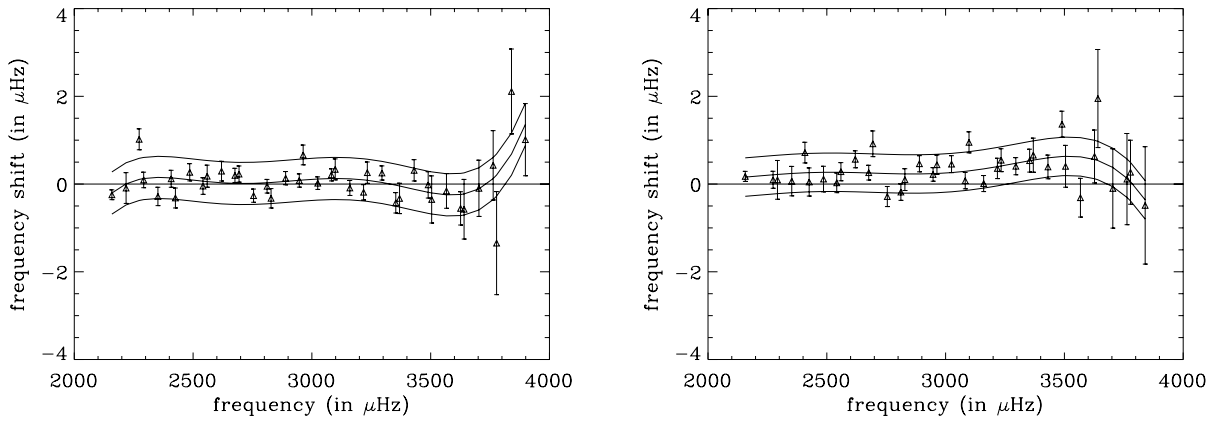

Fig. 1. The frequency asymmetry parameter $4a_2(n,l) - 10a_4(n,l)$ for $l = 2$ modes, plotted as a function of frequency, as measured by the Luminosity Oscillations Imager at low activity in 1996 (*left*), and at high activity in 2001 (*right*). The solid line in each panel is a smooth average through the fitted data (triangles with associated error bars), while the lower and upper lines show estimates of the 1σ uncertainties. Note that fits were made for several degrees, and the equivalent $l = 2$ a_2 and a_4 coefficients then derived as in Appourchaux et al. (2002).

equal to $4a_2(n,l) - 10a_4(n,l)$. Figure 1 shows the size of this asymmetry in frequency for observations performed in intensity by the Luminosity Oscillations Imager (Appourchaux et al. 1997) on SOHO. This frequency asymmetry parameter is an upper limit on the difference between the $\nu^{\rm FD}_{n,l}$ and $\nu^{\rm RES}_{n,l}$ frequencies, provided the difference $\nu^{\rm FD}_{n,l} - \nu^{\rm RES}_{n,l}$ is small with respect to the mode linewidth, Γ, over the frequency range of interest. In what follows, we assume that $\nu^{\rm FD}_{n,l} - \nu^{\rm RES}_{n,l}$ is small in order to enable us to linearize the equations in our formalism. Furthermore, we assume that the usual approach to fitting Sun-as-a-star data has been adopted, in which no account is taken in the fitting models for the frequency asymmetry. This pragmatic approach must be taken with shorter datasets, where moderate resolution in frequency makes it difficult to extract reliably the frequency asymmetry.

2.1. Analytical expression of the C^l_i

Estimation of the mode frequencies usually involves use of Maximum Likelihood Estimators. The following quantity is minimized:

$$\ln L = -\int \left(\ln S_0(\nu) + \frac{S_{\rm in}(\nu)}{S_0(\nu)} \right) {\rm d}\nu, \tag{2}$$

where S_0 is the fitted profile, and $S_{\rm in}$ is the input or "true" profile. The integral is introduced because we assume that all points in the power spectrum are independent. (Note that the product becomes a summation when using the logarithm.)

In order to derive estimates of the C^l_i, our approach is to linearize, to first order, expressions for the mode profiles as a function of the difference $\nu^{\rm FD}_{n,l} - \nu^{\rm RES}_{n,l}$. Hereafter we assume that the fitted maximum power spectral density (or height) and linewidth are the same as the input profile parameters. We assume explicitly that the fitted Sun-as-a-star, or full-disc, frequency, $\nu^{\rm FD}$, is extracted from the minimization found by taking the derivative with respect to $\nu^{\rm FD}$. Moreover, we assume naively that only a single parameter is affected, i.e., the mode frequency. To find the minimum in $\ln L$ one needs to solve the following:

$$\int \frac{\partial S_0(\nu)}{\partial \nu^{\rm FD}} \left(\frac{S_0(\nu) - S_{\rm in}(\nu)}{S_0^2(\nu)} \right) {\rm d}\nu = 0. \tag{3}$$

Here we may express $S_{\rm in}(\nu)$ in functional form as the sum of a Lorentzian and flat background noise (B):

$$S_{\rm in}(\nu) = \sum_{m=-l,l,2} s_m L^m_{\rm in}(\nu) + B. \tag{4}$$

Each $L^i_{\rm in}$ is the original profile of each mode, and s_m is the relative visibility (in power) of each component within a multiplet. On the assumption that the asymmetries in frequency are small, we may expand each Lorentzian profile as a function of the fitted Lorentzian thus:

$$L^m_{\rm in}(\nu) = L^m_0(\nu) + (\nu^{\rm RES}_{l,m} - \nu^{\rm FD}_{l,m}) \frac{\partial L^m_0(\nu)}{\partial \nu^{\rm FD}}. \tag{5}$$

Substitution of Eq. (5) into Eq. (4) gives:

$$S_{\rm in}(\nu) = \sum_{m=-l,l,2} s_m L^m_0(\nu) + B + \sum_{m=-l,l,2} s_m (\nu^{\rm RES}_{l,m} - \nu^{\rm FD}_{l,m}) \frac{\partial L^m_0(\nu)}{\partial \nu^{\rm FD}}. \tag{6}$$

The first two terms on the right-hand side give, by definition, $S_0(\nu)$; so, we have explicitly:

$$S_{\rm in}(\nu) = S_0(\nu) + \sum_{m=-l,l,2} s_m (\nu^{\rm RES}_{l,m} - \nu^{\rm FD}_{l,m}) \frac{\partial L^m_0(\nu)}{\partial \nu^{\rm FD}}. \tag{7}$$

Next, we assume that the odd splitting coefficients returned by the Sun-as-a-star, full-disc data fits are the same as those given by the resolved, imaging data fits. In that case, the frequency difference can be written as

$$\nu^{\rm RES}_{n,l,m} - \nu^{\rm FD}_{n,l,m} = \nu^{\rm RES}_0 - \nu^{\rm FD}_0 + \sum_{i=2,4,6} \alpha^{l,m}_i a_i(n,l), \tag{8}$$

where $\alpha^{l,m}_i$ are coefficients derived from Eqs. (2), (3), (5)–(7), and (11)–(14) of Chaplin et al. (2004). Now, substitution of Eq. (8) into Eq. (7) gives:

$$\begin{aligned} S_{\rm in}(\nu) \;=\; & S_0(\nu) + (\nu^{\rm RES}_0 - \nu^{\rm FD}_0) \frac{\partial S_0(\nu)}{\partial \nu^{\rm FD}} \\ & + \sum_{i=2,4,6} a_i \left(\sum_{m=-l,l,2} s_m \alpha^{l,m}_i \frac{\partial L^m_0(\nu)}{\partial \nu^{\rm FD}} \right). \end{aligned} \tag{9}$$

Finally, substitution of Eq. (9) into Eq. (3), followed by solution of the equation, gives:

$$\nu^{\rm FD}_{n,l} = \nu^{\rm RES}_{n,l} + \sum_{i=2,4,6} a_i(n,l) C^l_i, \tag{10}$$

where the C_i^l are given by:

$$C_i^l = \mathcal{K} \int \left(\sum_{m=-l,l,2} s_m \alpha_i^{l,m} \frac{\partial L_0^m(\nu)}{\partial \nu^{\rm FD}} \right) \frac{\partial S_0(\nu)}{\partial \nu^{\rm FD}} \frac{1}{S_0^2(\nu)} {\rm d}\nu, \quad (11)$$

with

$$\mathcal{K} = \left[\int \left(\frac{\partial S_0(\nu)}{\partial \nu^{FD}} \right)^2 \frac{1}{S_0^2(\nu)} {\rm d}\nu \right]^{-1}. \quad (12)$$

2.2. The C_i^l coefficients for the $l = 2$ modes

At $l = 2$ we took the $\alpha_i^{l,m}$ coefficients given in Eqs. (5)–(7) of Chaplin et al. (2004). The s_m mode visibility coefficients are 1 for $m = \pm 2$, and s_2 for $m = 0$:

$$C_2^2 = \mathcal{K}(2\mathcal{A}_2 - 2 s_2 \mathcal{B}_2), \quad (13)$$

$$C_4^2 = \mathcal{K}(2\mathcal{A}_2 + 12 s_2 \mathcal{B}_2), \quad (14)$$

with

$$\mathcal{A}_2 = \int \left(\frac{\partial (L_0^2 + L_0^{-2})(\nu)}{\partial \nu^{\rm FD}} \right) \frac{\partial S_0(\nu)}{\partial \nu^{\rm FD}} \frac{1}{S_0^2(\nu)} {\rm d}\nu, \quad (15)$$

and

$$\mathcal{B}_2 = \int \left(\frac{\partial L_0^0(\nu)}{\partial \nu^{\rm FD}} \right) \frac{\partial S_0(\nu)}{\partial \nu^{\rm FD}} \frac{1}{S_0^2(\nu)} {\rm d}\nu. \quad (16)$$

2.3. The C_i^l coefficients for the $l = 3$ modes

At $l = 3$ we took the $\alpha_i^{l,m}$ coefficients given in Eqs. (11)–(14) of Chaplin et al. (2004). The s_m mode visibility visibility coefficients are 1 for $m = \pm 3$, and s_3 for $m = \pm 1$:

$$C_2^3 = \mathcal{K}(3\mathcal{A}_3 - 1.8 s_3 \mathcal{B}_3), \quad (17)$$

$$C_4^3 = \mathcal{K}(3\mathcal{A}_3 + s_3 \mathcal{B}_3), \quad (18)$$

$$C_6^3 = \mathcal{K}(3\mathcal{A}_3 + 45 s_3 \mathcal{B}_3), \quad (19)$$

with

$$\mathcal{A}_3 = \int \left(\frac{\partial (L_0^3 + L_0^{-3})(\nu)}{\partial \nu^{\rm FD}} \right) \frac{\partial S_0(\nu)}{\partial \nu^{\rm FD}} \frac{1}{S_0^2(\nu)} {\rm d}\nu, \quad (20)$$

and

$$\mathcal{B}_3 = \int \left(\frac{\partial (L_0^1 + L_0^{-1})(\nu)}{\partial \nu^{\rm FD}} \right) \frac{\partial S_0(\nu)}{\partial \nu^{\rm FD}} \frac{1}{S_0^2(\nu)} {\rm d}\nu. \quad (21)$$

2.4. Comparison with results from Monte-Carlo simulations

Figures 2 to 6 show plots of the C_i^l coefficients as a function of mode linewidth, as calculated by the final analytical expressions given in Sects. 2.2 and 2.3 above. Predictions for the BiSON Sun-as-a-star data are rendered in each panel as a dashed line, while predictions for the VIRGO/SPM Sun-as-a-star data are rendered in each panel as a solid line. The calculations were performed using the observed mode visibility coefficients, s_2 and s_3, for BiSON and VIRGO (see figure captions), and realistic height-to-background ratios.

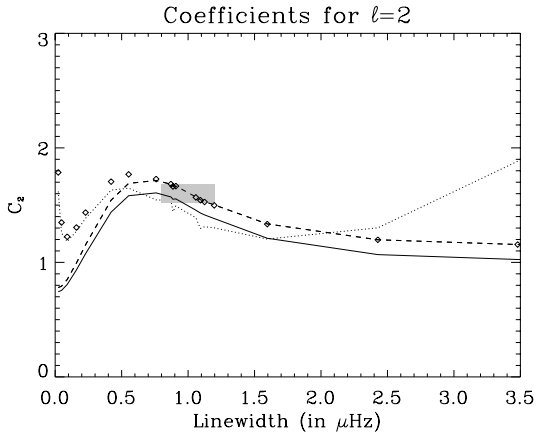

Fig. 2. C_2^2 coefficient as a function of linewidth for a mean frequency splitting of 0.4 μHz, an asymmetry of 0.2 μHz, and a realistic signal-to-noise ratio, for BiSON (dashed line) and VIRGO (heavy line) data. The coefficients derived from Monte-Carlo simulations of complete artificial BiSON-like p-mode spectra are plotted as the dotted line; while fits to spectra comprised of *isolated* $l = 2$ modes are plotted as diamond symbols. The light grey box represents the error bounds on the prediction of Chaplin et al. (2004). The visibility, s_2, for the $l = 2, m = 0$ mode is 0.54 for BiSON, and 0.65 for VIRGO.

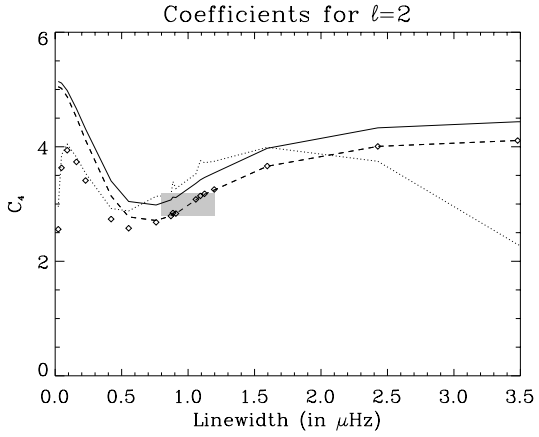

Fig. 3. C_4^2 coefficient as a function of linewidth for a mean frequency splitting of 0.4 μHz, an asymmetry of 0.2 μHz, and a realistic signal-to-noise ratio, for BiSON (dashed line) and VIRGO (heavy line) data. The coefficients derived from Monte-Carlo simulations of complete artificial BiSON-like p-mode spectra are plotted as the dotted line; while fits to spectra comprised of *isolated* $l = 2$ modes are plotted as diamond symbols. The light grey box represents the error bounds on the prediction of Chaplin et al. (2004). The visibility, s_2, for the $l = 2, m = 0$ mode is 0.54 for BiSON, and 0.65 for VIRGO.

The light grey box in each of Figs. 2 to 6 shows predictions given by Chaplin et al. (2004). They used results on fits to artificial BiSON-like Sun-as-a-star p-mode spectra, from which an average coefficient was determined by comparison of fitted and input frequencies for a range of modes.

We have also compared our new analytical predictions with predictions based on new results from Monte-Carlo simulations of artificial data. The trick in the Monte-Carlo simulations is to make artificial modes having underlying asymmetry of their components in frequency; but then to fit the modes to fitting models that take *no* account of the asymmetry. We generated results from two new sequences of simulations. In the first sequence, we made, and then fitted, complete artificial BiSON-like p-mode spectra. We fitted modes in the underlying limit spectra

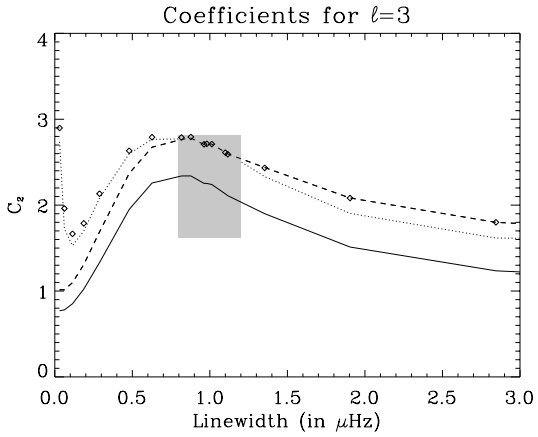

Fig. 4. C_2^3 coefficient as a function of linewidth for a mean frequency splitting of 0.4 μHz, an asymmetry of 0.2 μHz, and a realistic signal-to-noise ratio, for BiSON (dashed line) and VIRGO (heavy line) data. The coefficients derived from Monte-Carlo simulations of complete artificial BiSON-like p-mode spectra are plotted as the dotted line; while fits to spectra comprised of *isolated* $l = 3$ modes are plotted as diamond symbols. The light grey box represents the error bounds on the prediction of Chaplin et al. (2004). The visibility, s_3, for the $l = 3, m = \pm 1$ modes is 0.38 for BiSON, and 0.64 for VIRGO.

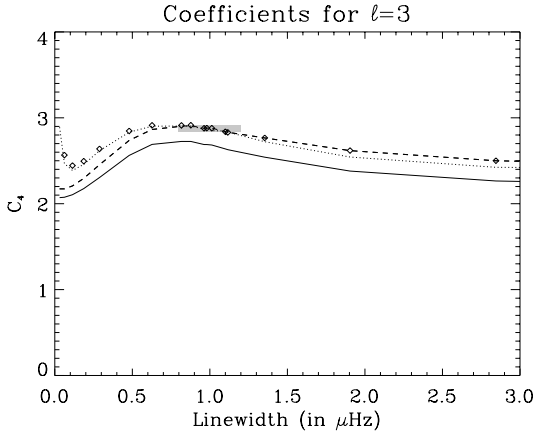

Fig. 5. C_4^3 coefficient as a function of linewidth for a mean frequency splitting of 0.4 μHz, an asymmetry of 0.2 μHz, and a realistic signal-to-noise ratio, for BiSON (dashed line) and VIRGO (heavy line) data. The coefficients derived from Monte-Carlo simulations of complete artificial BiSON-like p-mode spectra are plotted as the dotted line; while fits to spectra comprised of *isolated* $l = 3$ modes are plotted as diamond symbols. The light grey box represents the error bounds on the prediction of Chaplin et al. (2004). The visibility, s_3, for the $l = 3, m = \pm 1$ modes is 0.38 for BiSON, and 0.64 for VIRGO.

(i.e., with no realization noise) to get limit estimates of the C_i^l, again via comparison of the fitted and input frequencies. This approach, of using the limit spectrum, is presented and discussed in Toutain et al. (2005). The coefficients extracted from these artificial data are plotted in each panel of Figs. 2 to 6 as a dotted line.

For the second sequence of simulations, we fitted limit spectra comprised of *isolated* $l = 2$ or $l = 3$ modes. Results from these data are plotted as diamond symbols in Figs. 2 to 6. Results from the second sequence of simulations are seen to agree quite well with the analytical predictions over much of the plotted range in linewidth, Γ. Only at small values of Γ, where the assumption that $\nu_{n,l}^{\rm FD} - \nu_{n,l}^{\rm RES} \ll \Gamma$ breaks down, do the results begin to noticeably diverge.

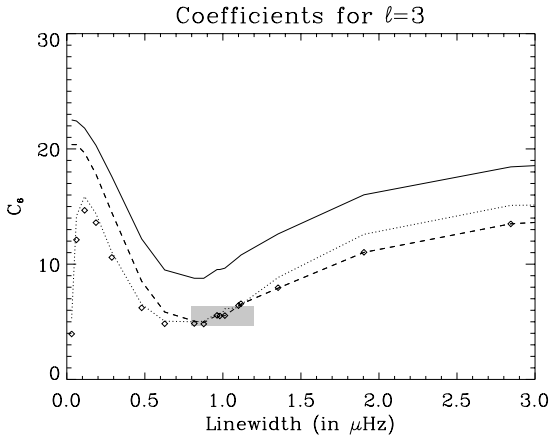

Fig. 6. C_6^3 coefficient as a function of linewidth for a mean frequency splitting of 0.4 μHz, an asymmetry of 0.2 μHz, and a realistic signal-to-noise ratio, for BiSON (dashed line) and VIRGO (heavy line) data. The coefficients derived from Monte-Carlo simulations of complete artificial BiSON-like p-mode spectra are plotted as the dotted line; while fits to spectra comprised of *isolated* $l = 3$ modes are plotted as diamond symbols. The light grey box represents the error bounds on the prediction of Chaplin et al. (2004). The visibility, s_3, for the $l = 3, m = \pm 1$ modes is 0.38 for BiSON, and 0.64 for VIRGO.

Inspection of the results from the first sequence of artificial data (dotted lines), which comprised complete BiSON-like p-mode spectra, give some idea of the impact of the cross-talk one might expect between neighbouring modes in a real, and crowded, Sun-as-a-star spectrum. The results from this first sequence broadly follow those of the analytical predictions, with the best agreement seen for the $l = 3$ data. That said, there are departures in detail.

3. Conclusion

It is clear that results from our analytical derivation approximate well the C_i^l coefficients derived from Monte-Carlo simulations of realistic, artificial, Sun-as-a-star p-mode data when the frequency asymmetry of components in a mode multiplet is small compared to the linewidth. This holds typically for a ratio of asymmetry-to-linewidth of less than ~0.3. For a larger ratio, Eq. (7) would need to be expanded to include higher-order terms. The derivation does then become a little cumbersome, and results on fits to artificial p-mode limit spectra may provide a more pragmatic route to deriving the C_i^l coefficients.

Acknowledgements. SOHO is a mission of international collaboration between ESA and NASA. We thank the referee (F. Pijpers) for his positive comments.

References

Appourchaux, T., Andersen, B., Fröhlich, C., et al. 1997, Sol. Phys., 170, 27
Appourchaux, T., Andersen, B., & Sekii, T. 2002, in From Solar Min to Max: half a solar cycle with SOHO, ed. C. Fröhlich, & A. Wilson (ESA SP-508, ESA Publications Division, Noordwijk, The Netherlands), 47
Chaplin, W. J., Elsworth, Y., Howe, R., et al. 1996, Sol. Phys., 168, 1
Chaplin, W. J., Appourchaux, T., Elsworth, Y., et al. 2004, A&A, 424, 713
Fröhlich, C., Romero, J., Roth, H., et al. 1995, Sol. Phys., 162, 101
Gabriel, A. H., Grec, G., Charra, J., et al. 1995, Sol. Phys., 162, 61
Harvey, J. W., Hill, F., Hubbard, R., et al. 1996, Science, 272, 1284
Scherrer, P. H., Bogart, R. S., Bush, R. I., et al. 1995, Sol. Phys., 162, 129
Toutain, T., Elsworth, Y., & Chaplin, W. J. 2005, A&A, 433, 713